

Dr. Imai is a member of the Optical Society of America, the Institute of Electronics and Communication Engineers of Japan, and the Japan Society of Applied Physics.

*



Tatsuyuki Ohashi received the B.S. and M.S. degrees in applied physics from Hokkaido University, Sapporo, Japan, in 1980 and 1982, respectively. When he was working in the M.S. degree he was engaged in fiber-optic sensors and measurements.

He is now with the Sakura Works, Fujikura Cable Ltd., Sakura, Japan.

Mr. Ohashi is a member of the Japan Society of Applied Physics.



Yoshihiro Ohtsuka graduated from Defence Academy, Yokosuka, Japan, in 1959. After two years at the Japan Defence Agency he became a graduate student in applied physics at Osaka University, Osaka, Japan, and received the M.S. and Ph.D. degrees in 1964 and 1968, respectively.

He was a Research Associate at the Department of Applied Physics, Faculty of Engineering, Osaka University, from 1964 to 1968 and also a member of the Research Fellow at the Institute of Plasma Physics, Nagoya University, Nagoya, Japan, from 1966 to 1968. In 1968 he was promoted to an Associate Professor at the Department of Engineering Science, Faculty of Engineering, Hokkaido University, Sapporo, Japan. From 1974 to 1975 he was with the research group on fiber optics at the Department of Electronics, University of Southampton, Southampton, England. Since 1977, he has been Professor of Faculty of Engineering at Hokkaido University and is working in optics related to laser physics and its applications.

Dr. Ohtsuka is a member of the Optical Society of America and the Japan Society of Applied Physics.

An External Cavity Diode Laser Sensor

RONALD O. MILES, MEMBER, IEEE, ANTHONY DANDRIDGE, ALAN B. TVETEN, AND
THOMAS G. GIALLORENZI, SENIOR MEMBER, IEEE

Abstract—A simple compact optical sensor system consisting of a near-field external cavity coupled to a semiconductor laser is reported. In this device, a change of phase in the light fed back into the laser cavity by the perturbed external mirror modulates the output of the laser by effectively changing the laser facet reflectivity. Phase shifts of $9 \cdot 10^{-8}$ rad and 10^{-6} rad were measured at 10 kHz and 100 Hz, respectively, using a 1-Hz bandwidth and a 98-percent reflector placed less than $10 \mu\text{m}$ from the laser facet. The sensitivity of these devices is shown to be limited by the intrinsic amplitude noise of the laser. The implementation of this sensor configuration is reported as an acoustic sensor, hydrophone, magnetic field, and current sensor as well as an accelerometer.

I. INTRODUCTION

ADVANCES in optical sensors have recently occurred primarily in fiber-optic systems. These devices sense either a change in phase or amplitude of the light propagating in the fiber due to a perturbation by an external field. Phase sensitive devices consist of single-mode fiber, generally, con-

figured in the form of a Mach-Zehnder-type interferometer with a reference arm and a signal arm [1]–[5]. Small changes in the phase of the light propagating in the signal arm are induced by an external field. When combined with the light in the unperturbed reference fiber at the detector, small changes in phase are easily detected. Such devices can be made increasingly sensitive by increasing the fiber-interaction lengths. Phase shifts on the order of a microradian have been detected with these sensors [4], [5].

Other fiber configurations sense changes in light transmission through the fiber. In this case, external fields create a waveguide loss which results in an intensity or amplitude variation in the output proportional to the applied signal [5]–[8]. Amplitude sensing devices are, in general, less sensitive than interferometer configured sensors [7], [8]. The advantage of this sensor is simplicity of construction and compatibility with multimode fibers. Fiber-optic sensors have been used to measure various environmental conditions. Recently, however, they have been constructed as magnetic field, temperature, current, acoustic, and acceleration sensors.

In this paper, we discuss recent developments of another sensor that is primarily a phase-sensing device, the external

Manuscript received September 9, 1982; revised October 22, 1982.
The authors are with the Naval Research Laboratory, Washington, DC 20375.

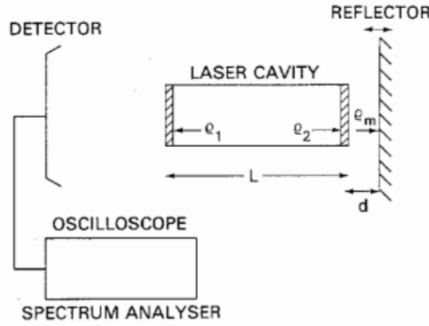


Fig. 1. Diagram of an external cavity laser diode sensor.

cavity diode laser or simply referred to as a laser diode sensor [9], [10]. A schematic diagram of this device is seen in Fig. 1. The laser diode sensor consists of a laser diode acting as a coherent light source tightly coupled to an external reflector where $d \ll L$. The presence of the external reflector creates a standing wave which alters the effective facet reflectivity of the laser diode source. A slight change in position of the external reflector alters the phase of the light reflected back into the laser cavity thus varying the effective laser facet reflectivity. The output is monitored by a large area photo-diode at the opposite output facet.

Because the sensitivity of the fiber interferometer sensor is proportional to the length of the fiber arms, the ultimate sensitivity of the diode laser sensor will be somewhat less than its fiber counterpart. Unlike the fiber system, the external cavity diode laser sensor is simple and quite easily packaged in a relatively small volume. The attributes of this device indicate a small, inexpensive package with microradian sensitivity and large dynamic range. While this device may be considered very much a point sensor due to its geometry, it is possible by using a fiber or other type of waveguide to attach the external mirror to the laser and to extend its interaction length and sensitivity. In this case, the sensor becomes sensitive to changes in the waveguide or fiber-transmission characteristics. In this extended configuration, it is possible to incorporate some of the desirable characteristics of the fiber sensors described above, such as flexibility and increased sensitivity. As in the case of fiber sensors, the laser diode sensor can be configured to sense acoustic waves, magnetic and electric fields, current, temperature, and acceleration.

II. THEORY AND OPERATION

A. Spectral Characteristics

In the configuration of Fig. 1, light is fed back into the diode laser cavity from the external reflector. The effects observed in large-dimension external cavity lasers where $d \gg L$, such as the presence of external cavity modes in the emission spectra and spectral narrowing from several megahertz to a few hundred kilohertz [11], are not observed in this configuration where $d \ll L$. Since the external cavity modes for these dimensions are spaced much farther apart than the gain profile for the laser cavity, their effects are minimal. The emission, however, remains on a single longitudinal mode with the output and frequency stability significantly improved. Photo-

graphs of the laser output at about $1.2 I_{th}$ is compared in Fig. 2(a) for the coupled and uncoupled cases, where coupling is to a 4-percent external reflector less than $5 \mu m$ from the laser facet. Accompanying this effect is an observed decrease in the linewidth by a few megahertz; as shown in Fig. 2(b) and an increased frequency stability appearing as a reduction in phase noise [12], [13], in the order of 5-10 dB.

B. Effective Reflectivity and Resonator Coupling

In the configuration of Fig. 3(a), the laser diode source is tightly coupled to an external reflector in a short cavity ($d \ll L$). The presence of an external mirror coupled to the laser within a few wavelengths effectively alters the reflectivity of the nearest laser facet. The equivalent diagram is shown in Fig. 3(b), where the influence of the external reflector is integrated in an expression for effective reflectivity, which is a function of λ and d . In this model, it is necessary to include an expression for the coupling of light from a planar reflector into the laser through an aperture. This model must also include an expression for the effective facet reflectivity as a function of phase angle, due to the presence and motion of a near-field reflector, as was done by Voumard *et al.* [14].

A second expression which adequately describes the laser power output above threshold in terms of effective facet reflectivity will describe the performance of the external cavity laser diode as a sensor.

Complex reflectivities for the field amplitudes are used to denote the diode (ρ_1, ρ_2) and external (ρ_m) mirrors, where all mirrors are assumed to be lossless. Since the external mirror is assumed to be tightly coupled to the laser and $d \ll L$, multiple reflections are possible. Therefore, in this model, it is also important to take into account beam divergence and spot size of the light emitted from ρ_2 . To do this, an individual coupling factor C_n at the n th reflection for ρ_2 must be included. ρ_e is obtained by summation of all the field contributions reflected back into the active region of the laser diode

$$\rho_e = \rho_2 - \frac{1 - R_2}{\rho_2} \sum_{n=1}^{\infty} C_n (-\rho_2 \rho_m \exp(2i\theta_R))^n \quad (1)$$

where

$$\theta_R = 2\pi L/\lambda \quad (2)$$

$$R_2 = |\rho_2|^2 = 0.32 \quad (3)$$

and

$$\rho_e = \sqrt{R_e} \exp(i\theta_e) \quad (4)$$

θ_R is the phase term corresponding to one external resonator length L_R at λ . θ_e is the effective phase change on reflection.

The coupling coefficient C_n is dependent upon the configuration of the external resonator and the emitting area of the laser diode. Losses are assumed mainly due to diffraction. No general expression describes all possible coupling configurations, however, Roess [15] has derived expressions for coupling from a rectangular aperture to planar reflectors in both the near- and far-field cases. His model is based on an unfolded equivalent resonator formed by the emitting area of the diode and its image separated by $2L_R$. Coupling for this configura-

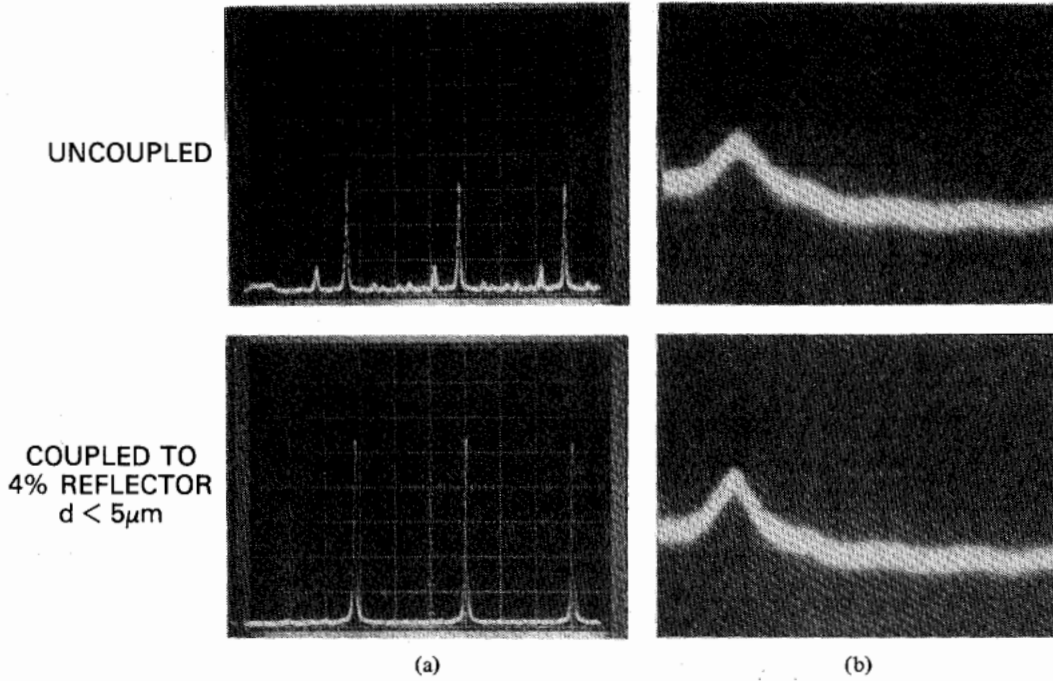


Fig. 2. (a) Emission spectra of a single-mode Hitachi HLP-1400 laser at $1.2 I_{th}$ for the uncoupled (free running) laser and the laser coupled to a 4-percent external reflector $< 5 \mu m$ from the laser facet. Data taken with a scanning Fabry-Pérot interferometer scanning 3 orders of spectral range. (b) Heterodyne line measurement technique showing narrowing on the order of a few MHz.

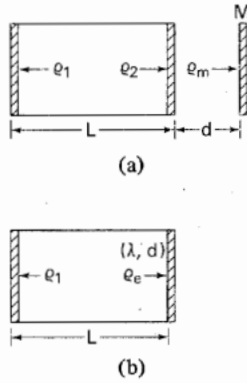


Fig. 3. Schematic representation of a diode laser coupled to an external cavity. (a) ρ_1 and ρ_2 are the complex reflectivities of the laser diode facets and ρ_m the reflectivity of the external mirror M . (b) $\rho_e(\lambda, d)$ is effective reflectivity of the laser facet influenced by the external reflector.

tion is by Fresnel diffraction where

$$F_a(L) = a^2/\lambda d \quad (5)$$

$$F_b(L) = b^2/\lambda d \quad (6)$$

are Fresnel numbers for the stripe aperture. $2a$ and $2b$ are the thickness and the width of the near-field spot size on the laser facet. For large Fresnel numbers where

$$F_a, F_b \gg 1$$

$$C_n = \{1 - 0.3[F_a(nd)]^{-3/2} - 0.3[F_b(nd)]^{-3/2}\}^{1/2}. \quad (7)$$

For small Fresnel numbers coupling losses can be estimated by

Fraunhofer diffraction, where

$$F_a, F_b \ll 1$$

$$C_n = \gamma[F_a(nd) \cdot F_b(nL)]. \quad (8)$$

γ is a geometric proportionality factor (for the diode laser = 0.072). In the case where

$$F_a < 0.8 \text{ and } F_b > 0.8.$$

The coupling coefficient is

$$C_n = (\gamma F_a(nd) \cdot \{1 - 0.3[F_b(nd)]^{-3/2}\})^{1/2}. \quad (9)$$

The dimensions of the spot size, $2a$, and $2b$ are critical in determining the coupling from the external reflector into the laser cavity. For devices using index-guided symmetric waveguides such as the buried heterostructure, the near-field spot size at the facet can be estimated from the far-field radiation pattern, using an approximate relationship developed by Botez [16]

$$w = B_d(0.31 + 3.15/D^{3/2} + 2/D^6), \quad 1.5 < D < 6 \quad (10)$$

where

$$D = \left(\frac{2\pi}{\lambda}\right) \cdot d(n_1^2 - n_2^2). \quad (11)$$

d is the thickness of the active layer and n_1, n_2 are the refractive indexes of the active layer and cladding layers, respectively. For lasers where the beam is guided by both the waveguide index and the gain distribution in the waveguide, (10) does not hold in all cases. Usually, to insure a single transverse mode, the beam is index guided in the direction transverse to the

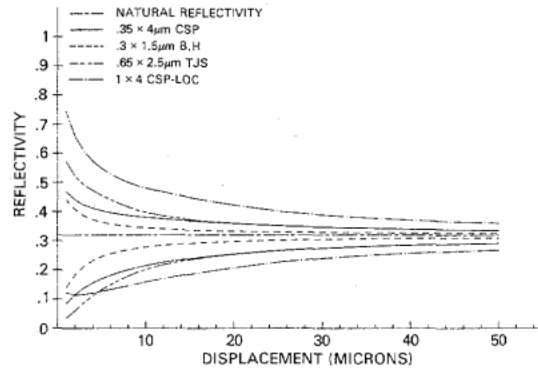


Fig. 4. Maxima and minima of the effective reflectivities of several lasers coupled to an external cavity as the coupling distance is varied from 1 to 50 μm . The effective aperture for each laser is listed.

TABLE I
NEAR-FIELD SPOT SIZE FOR SEVERAL COMMERCIALY
AVAILABLE LASER STRUCTURES

(The above data was obtained from the manufacturers in private communication.)

Laser type	2a μm	2b μm	Manufacturer
CSP	.35	4	Hitachi
CSP	.65	2.5	M/ACOM Laser Diode
CSP	1.0	4.0	M/ACOM Laser Diode LOC
B.H.	.3	1.5	Hitachi
TJS	.65	2.5	Mitsubishi

junction and, therefore, (10) can be applied. However, the width of the spot size (that dimension parallel to the junction) must be calculated from the solution of the waveguide modes for the near-field case or measured from the near-field spot size. A listing of the near-field spot sizes for several common laser structures which are potentially useful in various laser-diode-sensor applications, are given in Table I.

From (1) the effective reflectivity of the external cavity laser diode is seen to vary sinusoidally as a function of d . In Fig. 4, the maxima and minima of the effective reflectivity $R_e = \rho_e^2$ from (1) are plotted as a function of external cavity length, as d is varied from 1 to 50 μm . Various laser structures are compared. A high degree of coupling is assumed in each case ($N \geq 10$).

From Fig. 4 it is observed that large changes in effective reflectivity of the external cavity coupled laser occurs where d is varied within 10 μm of the laser facet and as expected, the laser with the largest near-field spot size shows the greatest variation in effective facet reflectivity. A plot showing the sinusoidal nature of the effective reflectivity as d is varied over 3 μm is shown in Fig. 5. A comparison is made showing the difference in output variation for the strongly coupled case where $n \geq 10$ and for a single pass where $n = 1$. With increased coupling, the presence of higher order harmonics tends to increase the slope of the transition between minima and maxima,

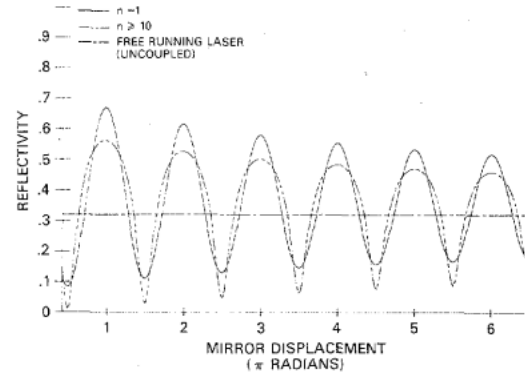


Fig. 5. Variation in effective facet reflectivity for the Hitachi CSP laser as coupling distance is continually increased over 3 μm . Comparison is made when the resonator is tightly coupled $n \geq 10$ and weakly coupled to $n \approx 1$.

while the periodicity remains unchanged. As coupling increases the output appears similar to a Fabry-Pérot interferometer with moderate fineness.

C. Laser Output Characteristics

An expression relating the laser output to mirror facet reflectivity can be found by considering the laser-rate equations and using a method outlined by Kato [17]. The laser-rate equations may be written

$$\frac{1}{c} \frac{dp}{dt} = (\sigma N - \gamma) P + A \frac{N}{\tau} \quad (13)$$

$$\frac{dN}{dt} = S - \left(\frac{1}{\tau} + P\sigma \right) N. \quad (14)$$

P is the photon flux density in the diode cavity, N is the population inversion density in the active region, σ is the stimulated emission cross section for the laser transition, γ is the loss coefficient, τ the lifetime of the injected free carriers, and A is the coupling coefficient of the spontaneous emission to the lasing mode. S is the pumping rate and is related to the threshold current density by the expression

$$S = \frac{2\eta}{qd} j \quad (15)$$

where η is the quantum efficiency, q the unit charge, d the thickness of the active layer, and j is the forward-driving current density. The loss coefficient γ may be expressed in terms of internal absorption and output-coupling losses

$$\gamma = \gamma_i + \frac{1}{L} \ln(1/R) \quad (16)$$

where γ_i is the internal loss term and L the length of the laser cavity. R is the combined reflectivity of the end facets where $R = R_1 R_2$.

The solution of (14) indicates that the population inversion increases with current density until threshold is reached. At that point, N approaches its asymptotic value $N_{th} = \gamma/\sigma$. Assuming only negligible amounts of spontaneous emission are coupled into the lasing mode after threshold is reached ($A \ll 1$), then the pumping rate approaches $S = \gamma/\sigma\tau$. When

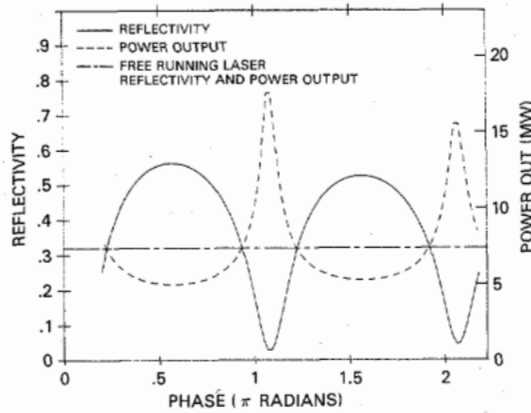


Fig. 6. Comparison of effective reflectivity and output power for the Hitachi CSP laser where the external resonator is located $10\ \mu\text{m}$ from laser facet and $I = 1.2 I_{\text{th}}$. Horizontal line represents uncoupled laser reflectivity and power.

this value and (16) are substituted into (15), an expression for the threshold current as a function of facet reflectivity can be written

$$J_{\text{th}} = \frac{qd}{2\sigma\tau\eta} \left(\gamma_i + \frac{1}{L} \ln(1/\sqrt{R_1 R_2}) \right) \quad (17)$$

when the quantum efficiency for the laser above threshold, η_s is known. The light output power of the laser can be written in terms of relative driving current $I_R = J/J_{\text{th}}$ and the threshold current density over the junction area $L \times W$

$$P_0 = \eta_0 L W J_{\text{th}} (I_R - 1) \quad (18)$$

since the facet reflectance R_2 can be replaced by the effective reflectance R_e calculated from (1). Equation (18) is an expression of the external cavity laser diode output in terms of known laser parameters and phase effects from the varying position of the external reflector. A plot of the effective reflectivity R_e and the output power calculated from (18) are shown in Fig. 6 as a function of external-cavity length over 2π rad. The parameters used to calculate the output power in Fig. 6 are for the Hitachi HLP 1400 driven at $1.2 I_{\text{th}}$ [17]–[20] where $d = 3.5 \cdot 10^{-5}$ cm, $\tau = 4 \cdot 10^{-9}$ s, $\sigma = 1.9 \cdot 10^{-17}$, $\eta = 0.51$, and $\gamma = 10$ cm $^{-1}$.

The light output characteristics as a function of current calculated from (18) are shown in Fig. 7. The change in lasing threshold is compared for the uncoupled laser (middle plot) and the coupled laser where light is fed back in phase (low threshold) and out of phase (high threshold), respectively. Also shown in Fig. 7 are the data from a Hitachi HLP-1400-CSP diode laser coupled to a 4-percent reflector placed $<10\ \mu\text{m}$ from the laser facet, where open and closed circles represent data points for light returned in phase and out of phase, respectively. Since actual experimental conditions were not precisely known, the calculated results are somewhat arbitrary. However, in this case, the calculated values seem to agree well with the experimental values when $n \approx 1$. The difference in slope of the output characteristics between the calculated and observed data is thought to be due to the dependence of the quantum efficiency of the device on optical feedback. This dependency was not included in the model.

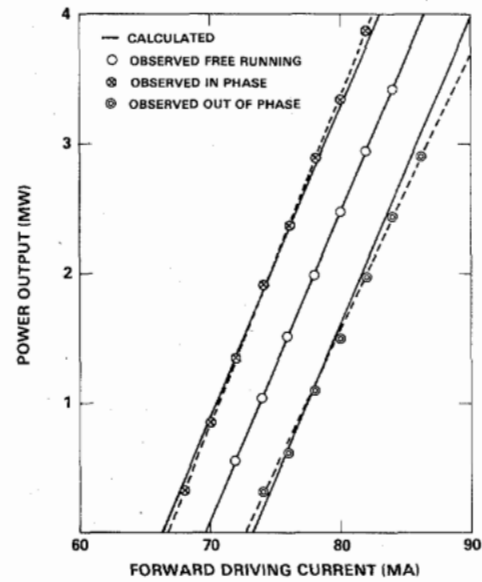


Fig. 7. Light output characteristics as a function of current from (18). Middle plot is the uncoupled laser characteristics. Lower and higher threshold characteristics shown for light fed back in phase and out of phase, respectively, $d < 10\ \mu\text{m}$. Open and closed circles represent data points for HLP-1400 laser coupled to a 4-percent reflector $<10\ \mu\text{m}$ from facet.

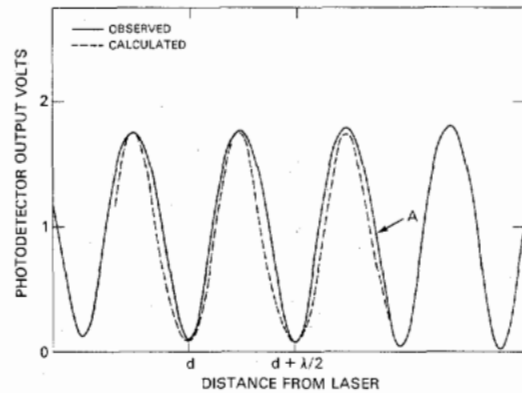


Fig. 8. Laser-diode-sensor output as a function of external reflector distance from laser facet displaying a $\lambda/2$ periodicity. Reflector position for maximum sensitivity is indicated by point A.

In Fig. 8, the output for the same laser is shown when a 98-percent reflector is placed within $10\ \mu\text{m}$ of the laser facet and continuously moved away. The laser output varied sinusoidally with a periodicity of $\lambda/2$ corresponding to a π -rad phase shift in the movement of the external reflector. Shown in the same figure is the calculated response using (18), where the best fit for the experimental data was for the weakly coupled case, where $n = 1$.

The external reflector can be optimally positioned for sensitivity by moving it until the output amplitude corresponds to point A in Fig. 8. At this point the output corresponds to the uncoupled laser. Slight movements of the reflector in any direction produce substantial changes in the output intensity of the laser. Obviously as the external mirror is more tightly coupled to the laser, as in Fig. 9, the slope of the laser response

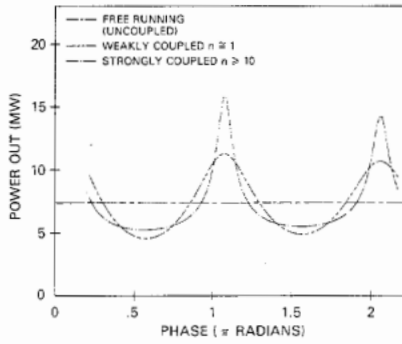


Fig. 9. Calculated laser-diode-sensor output as a function of external reflector distance from the laser facet. Comparison is made between the output of a strong and weakly coupled external reflector.

increases, augmenting the sensitivity of the laser output to the external reflector motion.

The sensitivity of this device as a motion sensor (where motion in the external reflector can be induced by several types of external fields) is determined first by the magnitude of the movement of the reflector to the incident field and second by the amplitude of the combined noise sources. The noise floor of the laser source is determined by a number of noise sources such as quantum shot noise, intensity noise, and phase noise, which are a result of fundamental properties of the laser. Thermal noise of the detector should also be considered as well as contributions from the external cavity structure. In general, the sensitivity depends on the resultant amplitude of these noise sources relative to the slope of the resonator response curve. For example, phase noise due to the frequency instability of the laser, scales directly with the slope of the response curve, as the origin of this noise is interferometric. It should also be noted that the intensity and phase noise has a $1/f$ frequency dependence [12], [13] while detector shot noise and thermal noise are independent of frequency. A short discussion of these predominant noise sources follows.

D. Noise Characteristics

1) *Shot Noise*: The noise voltage developed across the load resistor R of the photodetector (run photoconductively) by the current is given by

$$dV_s = \sqrt{2qV_0\Delta f R} \quad (19)$$

where q is the electronic charge, Δf the bandwidth, and V_0 the dc voltage across the load resistance.

The sensor's output V is approximately of the form

$$V \approx V_0(1 + \sin 2\phi) \quad (20)$$

where $\phi = 2\pi d/\lambda$ is the phase shift caused by the change in the facet/reflector distance d . At the maximum sensitivity position, the slope of the response curve is given by

$$\frac{dV}{d\phi} = 2V_0 \cos 2\phi = 2V_0 \quad (21)$$

thus the minimum detectable phase shift ϕ_s is given by

$$\phi_s = \frac{dV_s}{2V_0} \quad (22)$$

where V_0 is the dc output of the sensor at maximum sensitivity; this analysis assumes a 100-percent fringe visibility. Typically R was 10 k Ω and $V_0 = 3.5$ V, (these values are used in all subsequent calculations). For these values, the shot noise limited rms phase shift ϕ_s is $\sim 3 \times 10^{-8}$ rad; this corresponds to a reflector movement of $\sim 4 \times 10^{-6}$ nm.

2) *Intensity Noise*: The noise voltage dV_I caused by the laser's intensity noise dI , is related to the minimum detectable phase shift ϕ_I by

$$\phi_I = \frac{dV_I}{2V_0} \quad (23)$$

For the low-noise lasers studied in this work, $dV_I \sim 2$ - μ V rms for a 1-Hz band centered at 1 kHz, therefore, $\phi_I \sim 3 \times 10^{-7}$ rad.

3) *Phase Noise*: At the maximum sensitivity point for small frequency excursions of the laser (such that the interferometer responds linearly), the output of the sensor dV_F is given by

$$dV_F = 2V_0 \left(\frac{2\pi d}{c} \right) dv \quad (24)$$

where dv is the rms frequency fluctuation and c is the free-space velocity of light. Thus the phase noise-limited phase shift ϕ_F is given by

$$\phi_F = \left(\frac{2\pi d}{c} \right) dv \quad (25)$$

thus for typical values of d (~ 10 μ m) and dv (~ 10 kHz), ϕ_F is $\sim 2 \times 10^{-9}$ rad at 1 kHz.

4) *Thermal Noise*: The thermal noise of the load resistance is given by the standard Johnson noise equation and corresponds to approximately a minimum phase shift ϕ_T of $\sim 2 \times 10^{-9}$ rad.

The limiting minimum phase combining all of the listed sources of noise can be expressed as

$$\phi^2 = \phi_s^2 + \phi_I^2 + \phi_F^2 + \phi_T^2 \quad (26)$$

Obviously, from the discussion above, the chief source of noise in most laser-diode-sensor configurations will be the laser intensity noise. All other noise sources are nearly 2 orders of magnitude less. It becomes obvious then that one of the major criteria in the design of the external cavity laser diode sensor is a source with low intensity noise.

The actual measured minimum detectable phase shift ϕ_m varies from the ideal calculated value ϕ_c as a function of fringe visibility V or modulation depth, such that $\phi_m = V\phi_c$ where

$$V = \frac{V_{\max} - V_{\min}}{V_{\max} + V_{\min}} \quad (27)$$

and V_{\max} is the maximum detector voltage and V_{\min} the minimum. It has been assumed in previous calculations for minimum detectable phase shifts that $V = 1$. Typically, V was on the order of 0.90 or greater.

The modulation depth of this device is dependent upon the operating point of the laser output characteristics (Fig. 7) as well as the amount of light coupled back into the laser. A high degree of coupling insures a maximum threshold shift. The

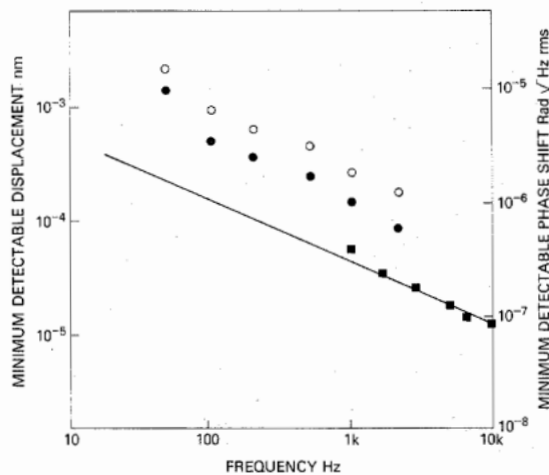


Fig. 10. Variation of the minimum detectable displacement and equivalent phase shift with frequency; (○) 4- and (●) 98-percent external reflector. The solid line indicates amplitude noise of low-noise CSP laser, (■) corresponding minimum displacement for coupled sensor device.

laser-output operating point is selected by increasing the driving current above threshold until V_{\min} rises slightly above threshold. It is desirable that the laser operate substantially above the free-running threshold to insure a good signal-to-noise ratio, since amplitude noise has been shown to decrease with forward-driving current [22].

In general, any misalignment of the external resonator cavity causes decoupling substantially reducing V . Mechanical resonances in the external cavity structure appear as discrete frequencies in the frequency-response spectrum of the sensor. By proper engineering design, such resonances can usually be designed to occur well out of the spectral region of interest.

Measurements of the minimum detectable movement of the reflector for the sensor system, diagramed in Fig. 1, were made by mounting the reflector on a piezoelectric element to allow a dc adjustment for maximum sensitivity, and to apply a signal to the position of the external reflector. Using a spectrum analyzer, the frequency dependence of the minimum detectable displacement for the HLP-1400 laser diode with a 4 and a 98-percent external reflector, placed less than $10 \mu\text{m}$ from the laser facet, was recorded and is shown in Fig. 10. Displacements of about $3 \cdot 10^{-4}$ and $9 \cdot 10^{-5}$ nm were measured at 100 Hz and 2 kHz, respectively, with a 1-Hz bandwidth for a 98-percent reflector. It is important to note that all sensors discussed in the remainder of this paper were limited to this sensitivity. However, recently measured improvements in the amplitude noise level of new low-noise CSP lasers, not yet commercially available, provide a factor-of-4 improvement in sensitivity.

Shown also in Fig. 10 is the amplitude noise of a low-noise uncoupled laser (solid line) and the corresponding minimum detectable signal of a sensor using this laser as a source. The corresponding $(f)^{-1/2}$ dependence of the amplitude noise of the uncoupled laser and the minimum detectable signal in the coupled-laser device indicate these devices are limited by the intrinsic amplitude noise of the laser.

The dynamic range of this sensor is limited by the minimum detectable phase shift (approximately 10^{-6} rad) and the maxi-

mum phase shift which is determined by the allowed nonlinearity of the sensor response (chosen to be approximately 0.1 rad). Thus the dynamic range is approximately 10^5 . This may be increased using an active feedback circuit to lock the sensor to the point of maximum sensitivity (phase-locked loop). In this case, when the voltage output of the photo detector drifts from the preset value for maximum sensitivity, an error voltage is fed back to the piezoelectric which corrects the position of the mirror [21]. With sufficient gain in the electrical feedback loop, the maximum phase shift may be increased to about π rad (dependent upon the frequency). Consequently, at low frequencies, a dynamic range of 10^7 should be obtainable.

The implementation of these principles outlined above to an actual device was found to be rather straight forward. Several rudimentary sensor configurations were constructed and tested. The simplicity of these devices was impressive, but in most cases further design engineering is required to rid them of unwanted resonances. In some cases, schematic diagrams along with an actual photograph of the device are shown with the response data for the device.

III. SENSOR CONFIGURATIONS

A. Acoustic Sensor

An external cavity diode laser can be configured as an acoustic sensor by using a thin plyable glass membrane either coated or uncoated, as an external reflector. An acoustic pressure wave, incident on the membrane, modulates the reflector position with respect to the laser facet, producing a change in phase of the optical feedback, which is then measured as an intensity modulation by the photoconductor. When the external reflector is tightly coupled, the motion of the reflector is along the direction perpendicular to the plane of the laser facet (x). It is assumed that the displacement is a linear function of pressure such that $\Delta x = \beta \Delta p$. This configuration requires that the thin membrane is mounted such that it has an adequate frequency response free of mechanical resonances over the frequency region of interest. The laser facet need not be anti-reflection coated to produce good results.

A photograph of a laboratory device is shown in Fig. 11. The laser is mounted on an orthogonal gimbal to provide the required alignment for good coupling with the external reflector. A piezoelectric cylinder positions the laser providing a separation distance for maximum sensitivity. The operating point for maximum sensitivity is obtained by observing the output from the rear laser facet with a photodetector mounted inside of the piezoelectric cylinder. As the laser is moved closer to the reflector on output response similar to Figs. 6 and 8 is observed; and maximum sensitivity set. The position of maximum sensitivity, referred to as quadrature, can be easily maintained by means of an active feedback circuit connected between the photodetector and the piezoelectric cylinder.

A typical response is shown in Fig. 12, where a calibrated constant output acoustic source was used to drive the acoustic sensor. The device's response was similar over four orders of magnitude of acoustic sensitivity. A number of resonances

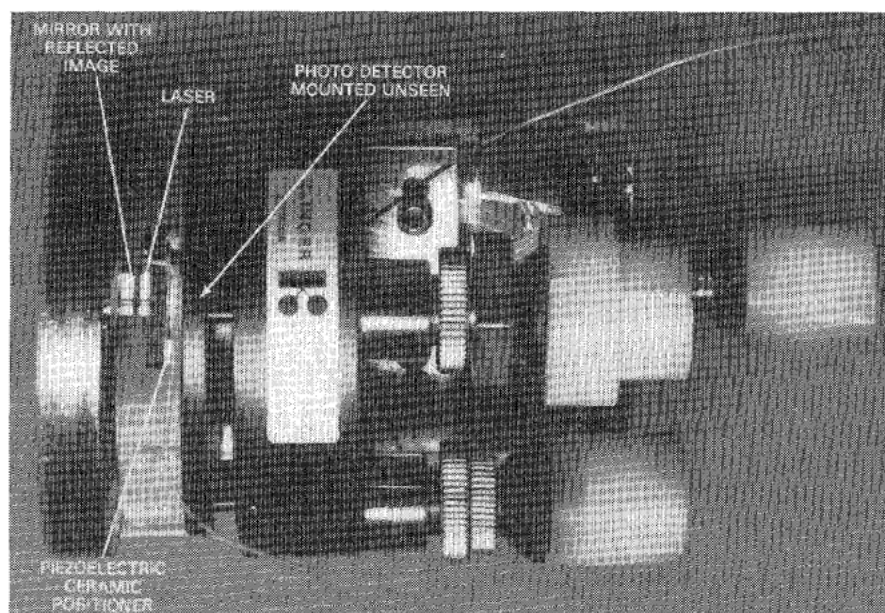


Fig. 11. Photograph of a laser diode acoustic sensor.

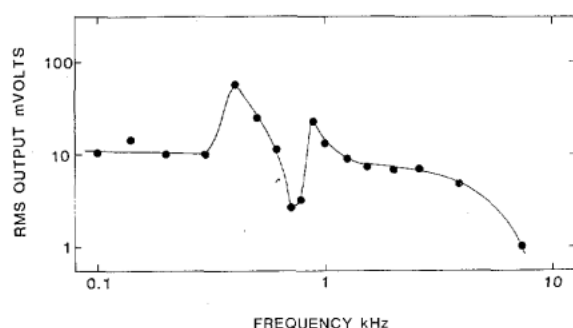


Fig. 12. Frequency response of the diode laser acoustic sensor.

(attributed to vibration resonances of the flexible glass membrane) were noted. Careful design of the membrane will be necessary to move the resonances to higher frequencies yet still maintain a high degree of sensitivity. The minimum detectable signal as a function of frequency for this device is seen in Fig. 10. The sensor interaction area can be increased somewhat in an alternative cavity configuration where a fiber-coupled reflector is used for the extended cavity.

B. Hydrophone

A simple hydrophone has been constructed using a configuration similar to the acoustic sensor described previously. A photograph of the device, showing a partially disassembled view, is seen in Fig. 13. This device was made considerably smaller than the previous laboratory acoustic sensor. Coupling alignment of the diode laser and external reflector is achieved by 3 alignment screws orthogonally mounted. Maximum sensitivity is set with the piezoelectric cylinder. The entire mechanical configuration was immersed in castor oil and the housing pumped down to prevent air bubbles from forming in the oil. A flexible reflective membrane of gold-coated mylar, 1 mil thick, was used as the reflector and interface with the

water. A small hole 0.2 mm in diameter was drilled in the side of the housing to serve as a means of balance the static pressure on either side of the membrane. The hole size was designed such that its resonant frequency would be well above the frequency region of interest. The configuration is shown schematically in the insert in Fig. 14. The response to underwater acoustic waves for a device similar to the one shown in Fig. 13 is shown in Fig. 14.

C. Magnetic Sensor

In this sensor, the reflector is attached to an element whose magnetic properties are such that the presence of a magnetic field displaces the reflector, with the displacement being proportional to the magnetic-field strength. One simple method of achieving this result is shown in Fig. 15. The modulation of the reflector position is achieved by mounting the reflector on one end of a short piece of thin-walled nickel tubing. The other end is attached to a piezoelectric element which is securely fixed to the substrate on which the laser is mounted. As with the sensors previously described, this device is kept at maximum sensitivity by adjusting the voltage on the piezoelectric element.

In this type of sensor, the term of interest is the first-order sensitivity of the function which relates the change in the magnetostriction to the applied time-varying magnetic field H_1 and the applied bias field H_0 . By analysis of the $\Delta l/l$ versus magnetic-field strength curves for various materials, it is possible to identify regions of steep slope in which a small change of ΔH results in a maximum dimensional change in $\Delta l/l$. For pure Ni, the bias field at which this change in length is a maximum is 3 G. At this bias-field strength $\Delta l/l = 2.9 \times 10^{-6} H_1$, where H_1 is measured in gauss. Consequently, if a 1-cm Ni tube is used then $\Delta L = 2.9 \times 10^{-8}$ m for a 1-G magnetic-field, this displacement would result in a 0.22-rad phase change. Therefore, if a 2×10^{-6} rad phase shift were desirable then

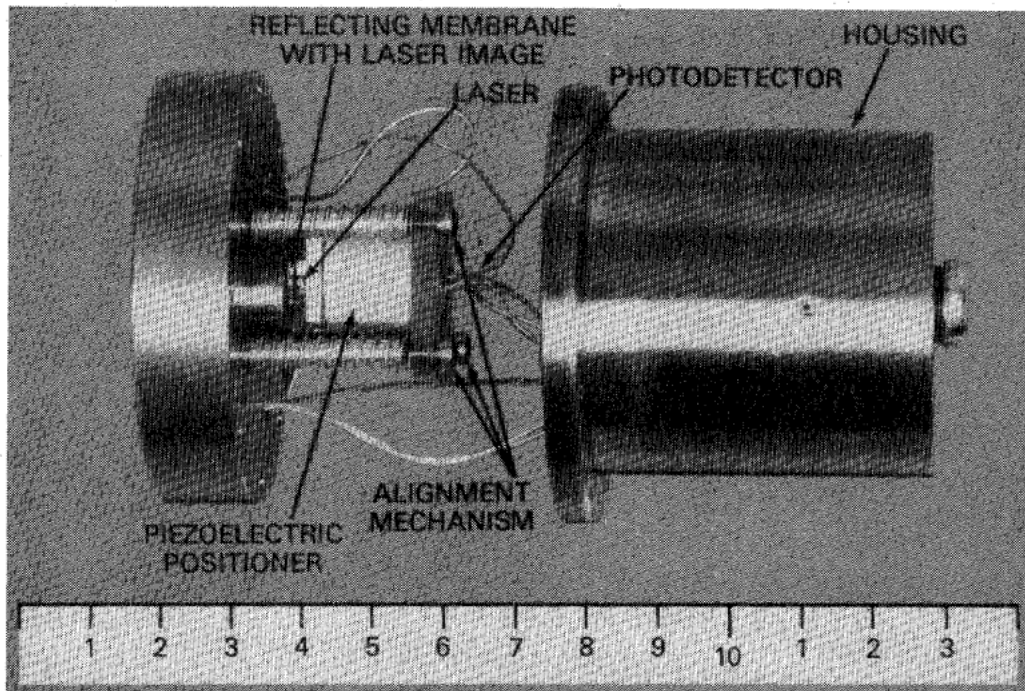


Fig. 13. Photograph of a laser diode sensor in a hydrophone configuration.

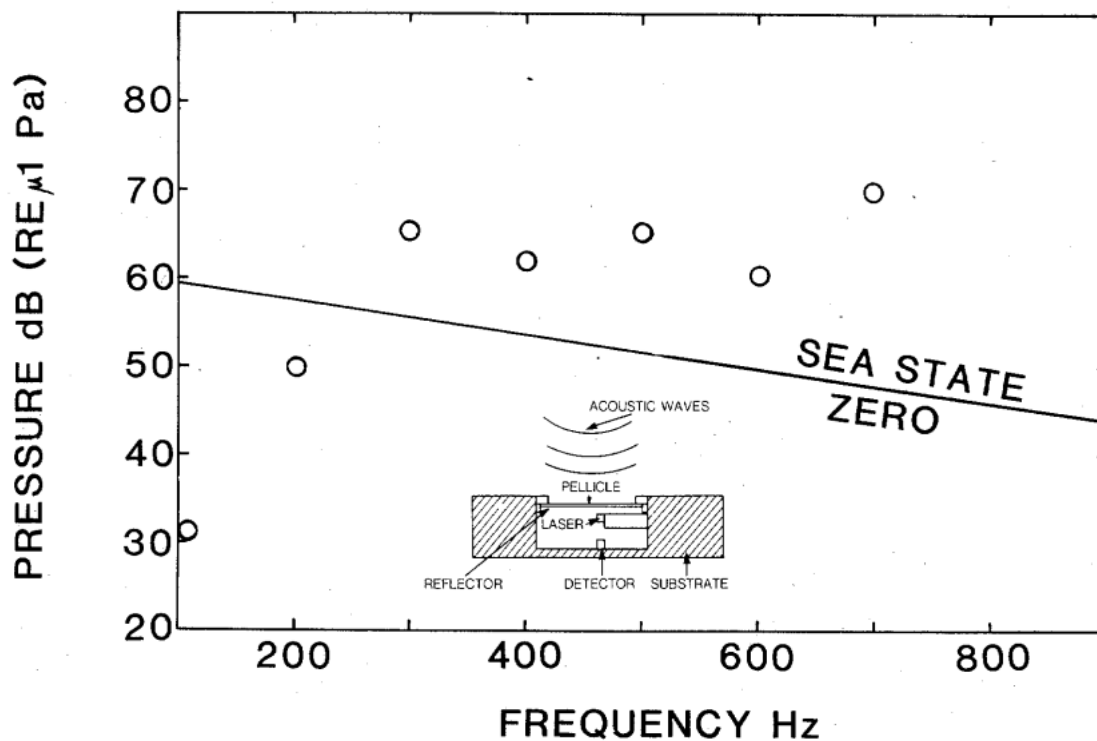


Fig. 14. Frequency response of a laser diode sensor configured hydrophone. Insert shows schematic representation of sensor.

the minimum detectable magnetic field would be 10^{-5} G. By constructing the magnetostrictive translation element from material with a larger magnetostrictive constant, such as metallic glasses, sensitivities may be increased by one or two orders of magnitude.

The frequency response of the sensor is shown in Fig. 16, at

these bias magnetic-field strengths. The frequency response was flat up to approximately 900 Hz, where the resonance of a part of the structure supporting the Ni tube is observed. The longitudinal resonance of the Ni tube itself was calculated to be about 10 kHz. The nickel tube was annealed to remove residual internal stresses prior to the sensor's construction.

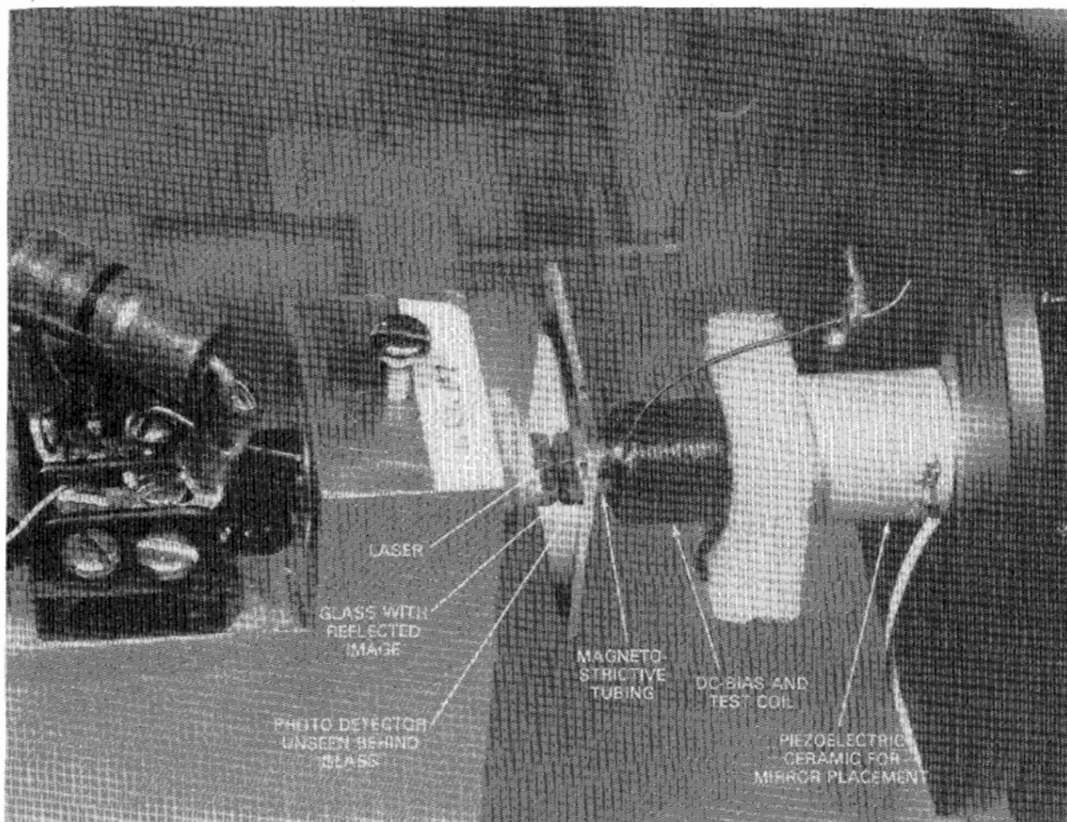


Fig. 15. Photograph of the laser diode magnetic sensor.

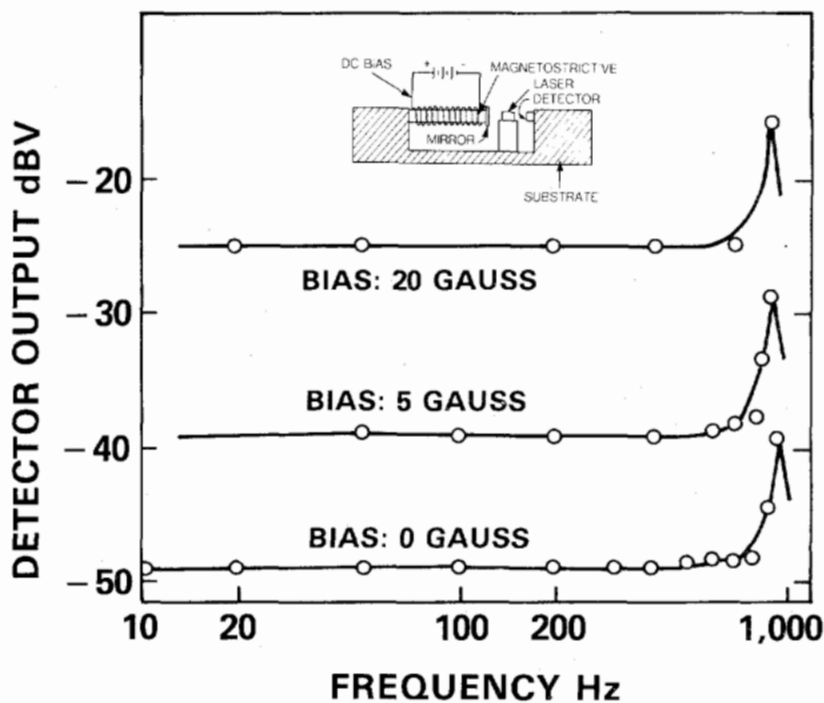


Fig. 16. Frequency response of the laser diode magnetic sensor. Results are shown for three different dc magnetic bias fields.

The measured sensitivity at 500 Hz, i.e., below the lowest resonant frequency, was 4×10^{-5} G, whereas the predicted sensitivity was approximately 6×10^{-6} G. It should also be noted that the bias field required for maximum sensitivity is 30 G,

which is approximately a factor of 10 greater than the 3 G published for pure Ni. It is known that the presence of small amounts of iron can expand the characteristic magnetostrictive curves of nickel along the magnetic-field axis. Impurities can

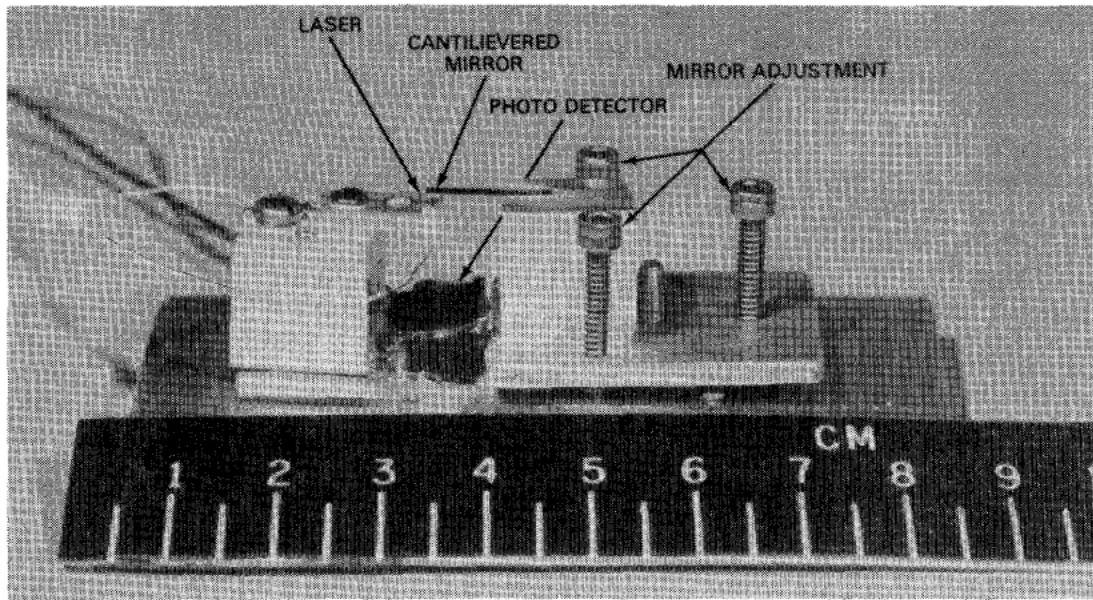


Fig. 17. Photograph of a laser-diode accelerometer.

also have the effect of reducing the relative length change thus reducing the magnetostrictive constant of the nickel. The observed sensitivity of the sensor and the large bias field are probably due to small amounts of impurity in the nickel used.

D. Current Sensor

The current sensor acts in a similar manner to the magnetic-field sensor. A coil of wire, through which the current to be detected is passed, is wrapped around the magnetostrictive element in the magnetic sensor described above. The sensor then detects the magnetic field associated with the current passing through the wire. Consequently, the frequency response curve is identical to that of the magnetic sensor; again a dc bias magnetic field is used to increase the sensitivity. The absolute sensitivity of the device is dependent on the coil configuration, but typically current in the 10^{-5} -10-A range may be measured.

E. Acceleration Sensor

The diode laser sensor was also configured to act as a sensitive single-axis accelerometer. A number of devices of different design have been constructed; a photograph of the simple design is shown in Fig. 17. The external reflector is mounted on a short 4-mm cantilever arm, the external reflector, approximately 1 mm^2 , also acts as the mass at the end of the cantilever. An acceleration along the axis of the laser cavity perturbs the position of the reflector from its rest position, thus producing the detectable phase shift. In the device shown, the maximum sensitivity position was achieved by adjustment of the screws shown. The stability was such that once adjusted the sensitivity remained constant for many minutes. In a practical device, a method of phase compensation would be required. The cantilever construction ensures that the device will not respond to cross-axis accelerations. A typical response of the 4-mm cantilever arm is shown in Fig. 18, the sensitivity in terms of rad/g is independent of frequency

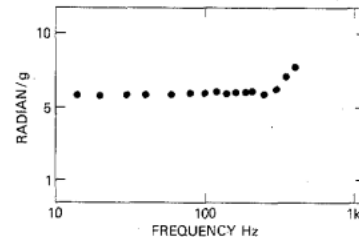


Fig. 18. Response of 4-mm cantilever arm.

below the resonance observed at $\sim 500 \text{ Hz}$. This value for the resonant frequency agrees with that calculated for the mechanical model described above. For this model, the resonant frequency varies inversely with the square root of the sensitivity. Therefore, an increase in the resonant frequency by a factor of two reduces the sensitivity by a factor of four. For any particular application, this relationship will determine the ultimate sensitivity of the device. Using the sensitivity of $\sim 5.8 \text{ rad/g}$ obtained from Fig. 18, a minimum detectable acceleration of $\sim 1 \mu\text{g}$ is calculated for a frequency of 100 Hz . As with the devices previously described, the sensor responded linearly to the magnitude of the applied acceleration over ~ 5 orders of magnitude.

IV. SUMMARY

In summary, we have discussed recent advancements in a new type of sensor. This sensor consists of an external reflector placed within a few wavelengths of the laser facet. This device senses a change in phase of the light fed back from the mirror as an external field perturbs its position with regard to the laser facet. These devices typically can measure a phase shift on the order of 10^{-6} rad with a dynamic range of 10^5 . When the reflector is well coupled to the laser cavity, the sensitivity of this device is dependent upon the magnitude of the movement of the mirror to the incident field and the amplitude noise of the laser source itself. In the devices tested

above, in nearly all cases, sensitivity was limited by the intrinsic amplitude noise of the laser. These devices can be configured to sense many varying fields and conditions. We have reported here the results of first effect sensors to measure acoustic fields as a microphone, and hydrophone, also a magnetic field sensor and current sensor, as well as an acceleration sensor.

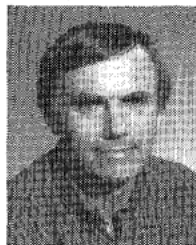
ACKNOWLEDGMENT

We wish to acknowledge and thank J. Cole and N. Lagakos for useful discussions and B. Danver for his help in testing the laser-diode-sensor hydrophone. We also wish to acknowledge L. Goldberg for the heterodyne-line measurement.

REFERENCES

- [1] J. A. Bucaro, H. D. Dardy, and E. Carome, "Fiber optic hydrophone," *J. Acoust. Soc. Amer.*, vol. 62, p. 1302, 1977.
- [2] J. H. Cole, T. G. Giallorenzi, and J. A. Bucaro, "Fiber interferometric demodulation and noise," in *FOC '81 East* (Boston, MA), Mar. 1981.
- [3] R. Hughes and J. Jarzynski, "Static pressure sensitivity amplification in interferometric fiber optic hydrophones," *Appl. Opt.*, vol. 19, p. 98, 1980.
- [4] D. A. Jackson, A. Dandridge, and S. K. Sheem, "Measurement of small phase shifts using a single-mode optical-fiber interferometer," *Opt. Lett.*, vol. 5, p. 139, 1980.
- [5] T. G. Giallorenzi, J. A. Bucaro, A. Dandridge, G. H. Sigel, Jr., J. H. Cole, S. C. Rashleigh, and R. G. Priest, "Optical fiber sensor technology," *IEEE J. Quantum Electron.*, vol. QE-18, pp. 626-665, Apr. 1982.
- [6] N. Lagakos, T. Litovitz, P. Macedo, and R. Meister, "Multimode optical fiber displacement sensor," *Appl. Opt.*, vol. 20, p. 167, 1981.
- [7] W. B. Spellman, Jr. and R. L. Gravel, "Moving fiber-optic hydrophone," *Opt. Lett.*, vol. 5, p. 30, 1980.
- [8] N. Lagakos, P. Macedo, T. Litovitz, R. Mohr, and R. Meister, "Fiber optic displacement sensor," in *Physics of Fibers*, vol. 2, Bernard Bendow and Shashanka S. Mitra, Eds; also *Advances in Ceramics*, vol. 539. Columbus, OH: American Ceramic Society, Inc., 1981.
- [9] A. Dandridge, R. O. Miles, and T. G. Giallorenzi, "Diode laser sensor," *Electron. Lett.*, vol. 16, p. 948, 1980.
- [10] R. O. Miles, A. Dandridge, A. B. Tveten, and T. G. Giallorenzi, "Fabry-Perot interferometric sensor," in *Proc. Conf. Integrated Opt. Fiber Commun. (IOOC'81)* (San Francisco, CA), Apr. 1981.
- [11] L. Goldberg, H. F. Taylor, A. Dandridge, J. F. Weller, and R. O. Miles, "Spectral characteristics of semiconductor lasers with optical feedback," *IEEE J. Quantum Electron.*, vol. QE-18, no. 4, 1982.
- [12] A. Dandridge, A. B. Tveten, R. O. Miles, D. A. Jackson, and T. G. Giallorenzi, "Single-mode diode laser phase noise," *Appl. Phys. Lett.*, vol. 38, p. 77, 1981.
- [13] E. Weidel and K. Peterman, "Semiconductor laser noise in an interferometer system," in *Proc. Conf. Integrated Opt. Fiber Commun. (IOOC'81)* (San Francisco, CA), Apr. 1981; also published in *IEEE J. Quantum Electron.*, vol. QE-17, p. 1251, 1981.
- [14] C. Voumard, R. Salathe, and H. Weber, "Resonance amplifier model describing diode lasers coupled to short external resonators," *Appl. Phys.*, vol. 12, pp. 369-378, 1977.
- [15] Roess, *Lasers Light Amplifiers and Oscillators*. New York: Academic, 1969, pp. 166-176; see also [14].
- [16] D. Botez, "Near and far-field analytical approximations for the fundamental mode in symmetric waveguide D.H. lasers," *RCA Rev.*, vol. 39, pp. 577-603, 1978.
- [17] D. Kato, "Minority-carrier lifetime reduction in the initial degradation of long life AlGaAs-AsGaAs lasers," *Appl. Phys. Lett.*, vol. 30, no. 12, pp. 642-643, 1977.
- [18] —, "High-reflectivity cavity mirrors for high-performance (GaAl) As diode lasers," *IEEE J. Quantum Electron.*, vol. QE-14, no. 8, pp. 563-565, Aug. 1978.
- [19] K. Aiki, M. Nakamura, T. Kuroda, J. Umeda, R. Ito, N. Chinone, and M. Maeda, "Transverse mode stabilized AlGaAs injection lasers with channeled-substrate-planar structure," *IEEE J. Quantum Electron.*, vol. QE-14, no. 2, pp. 89-94, Feb. 1978.
- [20] M. Nakamura and S. Tsuji, "Single-mode semiconductor injection lasers for optical fiber communications," *IEEE J. Quantum Electron.*, vol. QE-17, no. 6, pp. 994-1005, June 1981.
- [21] A. Dandridge and A. B. Tveten, "Phase compensation in interferometric fiber-optic sensors," *Opt. Lett.*, vol. 7, no. 6, pp. 279-281, June 1982.
- [22] R. O. Miles, A. Dandridge, A. B. Tveten, T. G. Giallorenzi, and H. F. Taylor, "Low frequency noise characteristics of channel substrate planar GaAlAs laser diodes," *Appl. Phys. Lett.*, vol. 38, no. 11, pp. 848-850, June 1, 1981.

*



Ronald O. Miles (S'66-M'77) was born in Salt Lake City, UT on November 25, 1940. He received the B.S. degree in electrical engineering, in 1967, and the M.S. and Ph.D. degrees, in 1973 and 1978, respectively, from the University of Utah, Salt Lake City, UT.

While at the University of Utah, his work included CO₂ laser plasma diagnostics and investigation of light in hollow-core waveguide lasers. In 1974, he was a consultant on preliminary design of gas dynamic laser for a laser-driven ionization process for applications in MHD power-generating systems for the Department of Electrical Engineering. From 1975 to 1976, he worked as a consultant on laser applications in development of new processes for preventive density for the Department of Mechanical Engineering. Since 1978, he has been at the Naval Research Laboratory, Washington, DC, where his research has dealt with noise and spectral properties of semiconductor lasers and fiber-optic sensor systems.

Dr. Miles is a member of the American Physical Society, the Optical Society of America, and Sigma Xi.

*



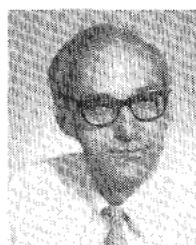
Anthony Dandridge was born in Kent, England on November 11, 1951. He received the B.S. and Ph.D. degrees in physics from the Sir John Cass School of Science and Technology, City of London Polytechnic, England.

His postgraduate and postdoctoral research work included flow birefringence, viscometric, and light-scattering studies of short-chain polymers. In 1979, he was a lecturer in Physics at the University of Kent, Canterbury, England.

Since 1980, he has been associated with Georgetown University, Washington, DC, John Carroll University, Cleveland, OH, and the Naval Research Laboratory, Washington, DC. His research work covers fiber-optic sensor systems as well as the noise and spectral characteristics of semiconductor lasers. He has authored and coauthored over 50 journal and conference publications.

Dr. Dandridge is a Fellow of the Royal Astronomical Society.

*



Alan B. Tveten was born in Wolf Point, MT on January 24, 1934. He received the B.A. degree from Concordia College, Moorhead, MN, the M.A. degree from the University of Nebraska, Lincoln, and the Ph.D. degree from Colorado State University, Fort Collins.

Before joining the Naval Research Laboratory, Washington, DC, in 1979, he worked as a Physics teacher at Dana College, Mankato State University, Mankato, MN and Colorado State University. He has done research in secondary electron emission in metals, magnetic susceptibility of rare earth oxides, and remote sensing using light scattering from aerosols. Since 1979, he has been working with the fiber-optic sensor and the optical information-processing groups at the Naval Research Laboratory, Washington, DC.



Thomas G. Giallorenzi (SM'78) was born in New York, NY, on February 28, 1943. He received the B.S. and M.S. degrees in engineering physics and the Ph.D. degree in applied physics from Cornell University, Ithaca, NY, in 1965, 1966, and 1969, respectively. At Cornell University, he worked on theoretical and experimental aspects of optical parametric scattering.

From 1969 to 1970, he was with the General Telephone and Electronics Laboratories, Inc., where his research was on plasma processes in gaseous lasers and arc lamps. In November 1970, he joined the Naval Research Laboratory,

Washington, DC. His research has included studies of Raman and parametric scattering, optical parametric oscillators, dye lasers, and fiber and integrated optics. From September 1977 to September 1979 he headed the Optical Techniques Branch. Since July 1979, he has headed the Optical Sciences Division which conducts research in all aspects of optical and electrooptical research. He has authored or coauthored over sixty journal publications and holds over twenty patents.

Dr. Giallorenzi is a member of the American Physical Society and the Optical Society of America. He received the Research Society of America Award for Applied Sciences in 1973 and the Navy's Meritorious Civilian Service Award in 1978.

Fiber-Optic Current and Voltage Sensors Using A $\text{Bi}_{12}\text{GeO}_{20}$ Single Crystal

KAZUO KYUMA, SHUICHI TAI, MASAHIRO NUNOSHITA, NOBORU MIKAMI, AND YOSHIKI IDA

Abstract—By using Faraday and Pockels' effects of a $\text{Bi}_{12}\text{GeO}_{20}$ (BGO) single crystal, two kinds of fiber-optic sensors for electric current and voltage were tentatively fabricated. The optimum design of these sensors and their performances were investigated. It was verified that the BGO crystal is very available for either of the current and voltage sensors with regard to their sensitivity and stability. As for the experimental results, the minimum detectable magnetic field of 10^{-2} Oe and the temperature dependence within ± 2 percent in the temperature range of -25 to 85°C was obtained for the current sensor, while for the voltage sensor the sensitivity of 10^{-3} V and the temperature dependence within ± 0.5 percent was in the same temperature range.

I. INTRODUCTION

A STRONG DEMAND for employing fiber-optic current and voltage sensors in electric power systems has been currently increased [1], together with the progress of fiber technologies. Attractive features of fibers [2], that is, good electrical isolation and immunity from electromagnetic interference, enable such sensors to control power systems remotely and securely. Many efforts to realize these sensors have been made by examining various kinds of magneto-optic (Faraday effect) [3]–[5] and electrooptic (Pockels' effect) materials [6], [7].

In this paper, an attempt to use $\text{Bi}_{12}\text{GeO}_{20}$ (BGO) single crystals, as the fiber-optic current and voltage sensors, was

TABLE I
ELECTRICAL AND OPTICAL PROPERTIES OF A $\text{Bi}_{12}\text{GeO}_{20}$ SINGLE CRYSTAL

Crystal form	** bcc-23
Magnetism	diamagnetics
Resistivity ρ	$10^{11} \sim 10^{13} \Omega\text{cm}$
Band-edge wavelength λ_g	$0.48 \mu\text{m}$
Refractive index* n_o	2.41
Electrooptic coefficient* γ_{41}	$3.1 \times 10^{-10} \text{ cm/V}$
Verdet constant* V_r	$0.188 \text{ min/Oe}\cdot\text{cm}$
Optical activity* θ	$9.6 \text{ deg}/\mu\text{m}$

* Optical properties are measured at the wavelength of $0.85 \mu\text{m}$.

** Body-centered-cubic structure.

performed. This BGO crystal was grown by the conventional Czochralski method [8] in our laboratory, and its electrical and optical properties measured are tabulated in Table I. The outstanding features of the BGO current and voltage sensors, fabricated here, are itemized as follows:

- 1) Since the BGO crystal has both remarkable Faraday and Pockels' effects, both the current and voltage sensors were constructed of a BGO cell.
- 2) These sensors, based on microoptics, are compatible with multimode fiber technologies.
- 3) Since the BGO single crystal has a body-centered cubic structure and has no natural birefringence, the current and voltage sensors have essentially very small temperature dependence of sensitivities.

Manuscript received September 14, 1982; revised January 3, 1983.

K. Kyuma, S. Tai, and M. Nunoshita are with the Central Research Laboratory, Mitsubishi Electric Corporation, Hyogo 661, Japan.

N. Mikami is with the Materials Engineering Laboratory, Mitsubishi Electric Corporation, Hyogo 661, Japan.

Y. Ida is with Itami Works, Mitsubishi Electric Corporation, Hyogo 661, Japan.